J. Fluid Mech. (1987), *vol.* 182, *pp.* 169–191
Printed in Great Britain

Three-dimensional numerical simulation of convection in low-Prandtl-number fluids

By M. MENEGUZZI
Service d'Astrophysique, Centre d'Etudes Nucléaires de Saclay, 91191 Gif sur Yvette and CNRS, France

C. SULEM
Department of Mathematics, Ben Gurion University of the Negev, Beersheva, Israel *and* CNRS, Centre de Mathématiques Appliquées, Ecole Normale Superieure, Paris, France

P. L. SULEM
School of Mathematical Sciences, Tel-Aviv University, Israel *and* CNRS, Observatoire de Nice, France

AND O. THUAL
Centre National de Recherche Météorologique, Météorologie Nationale, 31057, Toulousse-Cedex, France

(Received 16 October 1985 and in revised form 7 March 1987)

We present three-dimensional numerical simulations of convection in a low-Prandtl-number fluid confined between two infinite horizontal bounding surfaces maintained at constant temperatures. We consider the case of free-slip boundary conditions for a fluid of Prandtl number $Pr = 0.2$ and that of rigid boundary conditions with $Pr = 0.025$. In the former situation, we observe stationary, periodic, biperiodic and chaotic regimes as the Rayleigh number is increased. In the later situation, the dynamics involves very different characteristic times, and only stationary and time-periodic solutions have been simulated. Convergence to the later regime may occur after a long transient where the amplitude of the oscillation is slowly modulated.

1. Introduction

The investigation of convection in low-Prandtl-number fluids may have various motivations. These fluids are encountered both in industrial plants (liquid metals) and in astro- and geophysical situations. Furthermore, in connection with the development of the theory of dynamical systems, they are well adapted to study time-dependent convection: this regime arises as soon as the two-dimensional rolls become unstable (oscillatory instability) and temporal chaos occurs at a relatively low Rayleigh number when the geometry of the patterns is still simple. In this context, Libchaber & Maurer (1980) investigated experimentally convection in a small box of helium (Prandtl number $Pr = 0.1$) and observed a transition to chaos through a sequence of period-doubling bifurcations. Later, experiments were performed in mercury ($Pr = 0.025$) by Libchaber, Fauve & Laroche (1983). They investigated the effect of a magnetic field parallel to the rolls and observed different routes to chaos, depending on the intensity of the magnetic field and on the values of the aspect ratios.

The influence of lateral boundaries is generally not considered in theoretical or numerical investigations where periodicity is often imposed in the horizontal direction. On the upper and lower boundaries, the fluid is assumed either to slip freely (free-slip boundary conditions) or to be at rest (rigid boundary conditions). Rigid boundary conditions could appear more realistic, although quantitative comparison with experiments may be delicate because of the significant influence of lateral boundaries. On the other hand, the relative simplicity of free boundary conditions makes this situation more adapted to analytical investigation.

For free-slip, perfectly conducting overside and underside boundaries, Schlüter, Lortz & Busse (1965) computed analytically the steady solution corresponding to two-dimensional rolls for a Rayleigh number slightly in excess of the onset of convection R_c. The stability of this solution for low-Prandtl-Number fluids was discussed by Busse (1972) who found that these solutions are unstable to an oscillatory instability when the Rayleigh number exceeds a value R_{osc} whose distance from R_c tends to zero like Pr^2. This analysis seems valid when the horizontal periods are comparable with the depth of the flow, but has recently been questioned in the case where long-wavelength motions are permitted. In this case, the two-dimensional rolls may always be unstable at sufficiently low Prandtl number (Siggia & Zippelius 1981; Zippelius & Siggia 1982, 1983; Busse & Bolton 1984; Bolton & Busse 1985).

Rigid boundaries were considered by Clever & Busse (1974). Prescribing an horizontal periodicity corresponding to the most unstable wavenumber in this geometry ($k_x = 3.117$), they computed numerically the steady solution corresponding to two-dimensional rolls. They also analysed the linear stability of these solutions for three-dimensional disturbances and showed that at low Prandtl number, the dominant instability is the oscillatory instability. At $Pr = 0.025$, this instability occurs at $R_{osc} \approx 1885$. More recently, Busse & Clever (1983) investigated the stabilizing effect of a magnetic field parallel to the roll axis.

Numerical simulation of time-dependent convection was first performed in the case of two-dimensional flows satisfying free-slip boundary conditions (Moore & Weiss 1973 and references therein), at Rayleigh number up to 1000 times the critical value for the onset of convection. Prandtl numbers as small as 0.01 were considered. Two-dimensional oscillatory solutions were observed for $Pr > 1$. These solutions could be physically relevant when an external constraint (like a magnetic field) maintains the two-dimensionality, but are otherwise unstable relatively to three-dimensional perturbations.

Three-dimensional numerical simulations of time-dependent convection have been reported at moderated Prandtl numbers. For rigid boundary conditions and $Pr = 0.71$, Lipps (1976) observed the onset of steady convection and, at higher Rayleigh numbers, transition to time-dependent regimes with one or two frequencies. More recently, McLaughlin & Orszag (1982) observed the subsequent transition leading to a chaotic regime by a scenario which supports the theory of Ruelle, Takens & Newhouse (1982). For free-slip boundary conditions and Prandtl number of order one or larger, Curry *et al.* (1984) made a detailed comparison of convection in two and three dimensions. They also discussed the effect of an inadequate spatial resolution, which can lead to spurious time-dependence (see also Orszag & Kells 1980; Marcus 1981; Treve & Mauly 1982).

In this paper, we use very similar numerical methods to simulate convection in low-Prandtl-number fluids, in the two cases of free-slip boundary conditions at $Pr = 0.2$ and rigid boundary conditions at $Pr = 0.025$. Our aim is to investigate those aspects of transition to time-dependent convection, and eventually to chaos, that are

specific to low Prandtl numbers. The effect of a magnetic field parallel to the roll axis is also discussed.

Convection with free-slip boundary conditions at low Prandtl number ($Pr = 0.1$) was also considered by Herring & Jackson (1984) but in a different spirit. Using a Rayleigh number 70 times critical, they dealt with turbulent convection and focused their analysis (in particular comparison of direct simulation and closure calculations) on statistical qualities characteristic of developed turbulence.

2. The dynamical equations

We consider a horizontal fluid layer confined between two horizontal bounding plates and heated from below. The overside and underside planes are assumed to act as either rigid or as free-slip perfectly conducting boundaries. Periodicity is assumed in the horizontal directions. Let d denote the thickness of the layer. In the x-direction, we choose a period $L_x = 2\pi d/k_x$ corresponding to the most unstable mode; $k_x = \pi/\sqrt{2}$ for free-slip boundary conditions and $k_x = 3.117$ for rigid boundary conditions. In the y-direction, we use a period $L_y = 2\pi/k_y$ with $k_y = \pi/\sqrt{2}$ for free-slip conditions and $k_y = 2.5$ for rigid conditions.

To write the equations of motion in a non-dimensional form, the thickness d of the layer is taken as unit length. For the time unit, either the diffusive time d^2/κ or the viscous time d^2/ν is used. The later unit is useful at low Prandtl number. The temperature deviation ϑ from the diffusive profile is measured in units of ΔT or of $Pr\,\Delta T$, where ΔT is the temperature difference between the lower and upper boundaries.

In §7 we briefly consider the effect of an external magnetic field $\boldsymbol{B}_0$ (directed in the y-direction) on convection in a low magnetic Prandtl number conducting fluid (in mercury, $P_m \approx 10^{-6}$), assuming rigid boundary conditions. The induced magnetic field $\boldsymbol{b}$ is then weak compared with $\boldsymbol{B}_0$ and can be viewed as a slave variable, prescribed by the velocity field. In the limit $P_m \to 0$, the MHD–Boussinesq equations indeed reduce to the following system, where $\boldsymbol{b}$ is measured in unit of $B_0 P_m$, ϑ in units of $Pr\,\Delta T$ and t in units of d^2/ν (Roberts 1967; Sulem, Sulem & Thual 1985):

$$\left.\begin{aligned} \frac{\partial \boldsymbol{v}}{\partial t} + \boldsymbol{v}\cdot\nabla\boldsymbol{v} &= -\nabla^2\boldsymbol{v} + R\vartheta\boldsymbol{e}_3 + Q\frac{\partial \boldsymbol{b}}{\partial y} - \nabla p, \\ \nabla^2\boldsymbol{b} &= -\frac{\partial \boldsymbol{v}}{\partial y}; \quad \nabla\cdot\boldsymbol{v} = 0, \\ \frac{\partial \vartheta}{\partial t} + \boldsymbol{v}\cdot\nabla\vartheta &= \frac{1}{Pr}(\nabla^2\vartheta + v_3). \end{aligned}\right\} \tag{2.1}$$

$\boldsymbol{e}_3$ denotes the upward vertical unit vector; v_3 is the vertical component of velocity $\boldsymbol{v}$. The Rayleigh number R, the thermal Prandtl number Pr and the Chandrashekhar parameter Q are defined as

$$\left.\begin{aligned} R &= \alpha g \frac{\Delta T d^3}{\nu\kappa}, \\ Pr &= \frac{\nu}{\kappa}, \\ Q &= \frac{B_0^2 d^2}{(\rho_0 \lambda \nu)}, \end{aligned}\right\} \tag{2.2}$$

where g is the intensity of the gravity field and ρ_0 the mass of the unit volume. The transport coefficients ν, λ and κ are the kinematic viscosity, the magnetic diffusivity and the thermal diffusivity, respectively; α is the coefficient of thermal expansion.

Boundary conditions must be added to (2.1). On the horizintal boundary planes, the temperature deviation from the diffusive profile vanishes together with the normal component of the velocity. The tangential velocity component also vanishes in the case of rigid boundary conditions, while the tangential stress vanishes in the case of free-slip conditions. In addition, the normal component of the current $\boldsymbol{j} = \mathrm{Curl}\,\boldsymbol{b}$ vanishes (Roberts 1967). We thus have on the bounding planes $z = \pm\frac{1}{2}$:

$$\vartheta = v_3 = b_3 = \frac{\partial b_1}{\partial z} = \frac{\partial b_2}{\partial z} = 0 \tag{2.3}$$

and

$$\frac{\partial v_1}{\partial z} = \frac{\partial v_2}{\partial z} = 0 \quad \text{for free-slip conditions.} \tag{2.4a}$$

or

$$v_1 = v_2 = 0 \quad \text{for rigid conditions.} \tag{2.4b}$$

It could be suggested that the Boussinesq equations may be simplified in the limit of very small (thermal) Prandtl numbers by neglecting the Lagrangian derivative in the equation for the temperature fluctuations (2.1), making the buoyancy force linear in the vertical component of the velocity. This approximation may seem analogous to that done in the limit of small magnetic Prandtl numbers. The difference is that, while in MHD the Lorentz force gives a scale-independent dissipative term, the buoyancy force becomes a linear destabilizing term in the large scales which may lead to divergence of the solution because the nonlinear terms are not sufficient to stabilize the system (J. H. Herring, private communication). This may be related to the fact that, at large Rayleigh and small Prandtl numbers, the streamlines of two-dimensional convection flow tend to become circular and to coincide approximately with the lines of constant vorticity (Clever & Busse 1981; Busse & Clever 1981).

3. Computational techniques

3.1. *Free-slip boundary conditions*

We use a pseudospectral method where velocity and temperature are expanded in exponential Fourier series in the horizontal spatial variables and in cosine series (for the horizontal components) or sine series (for the vertical velocity component and the temperature), in the vertical direction, to take into account the boundary conditions (2.3) and (2.4a). For each of these functions, we have retained 24 modes for every horizontal direction and 12 modes for the vertical direction. For the Rayleigh numbers that we have considered, this resolution ensures that the truncation error is negligible: the excitation of the highest wavenumbers that are retained is comparable to the round-off error.

Concerning time-steps, we use (here t is measured in units of d^2/κ and ϑ in units of ΔT)

$$\frac{1}{2\delta t}(\hat{\boldsymbol{v}}_{\boldsymbol{k}}^{n+1} - \hat{\boldsymbol{v}}_{\boldsymbol{k}}^{n-1}\exp(-2\boldsymbol{k}^2\delta t)) = \mathbb{P}(\boldsymbol{k})(\boldsymbol{v}^n \times \boldsymbol{\omega}^n)_{\boldsymbol{k}} + \tfrac{1}{2}Re_3(\hat{\vartheta}_{\boldsymbol{k}}^{u-1}\exp(-2\boldsymbol{k}^2\delta t) + \hat{\vartheta}_{\boldsymbol{k}}^{n+1}) \tag{3.1a}$$

$$\frac{1}{2\delta t}\left(\hat{\vartheta}_{\boldsymbol{k}}^{n+1} - \hat{\vartheta}_{\boldsymbol{k}}^{n-1}\exp\left(\frac{2k^2}{Pr}\delta t\right)\right) = -(\boldsymbol{v}^n \cdot \boldsymbol{\nabla}\vartheta^n)_{\boldsymbol{k}}\exp\left(\frac{-2k^2}{Pr}\delta t\right) + \frac{1}{2}\left(\hat{v}_{3,\boldsymbol{k}}^{n-1}\exp\left(\frac{-2k^2}{Pr}\delta T\right) + \hat{v}_{3,\boldsymbol{k}}^{n+1}\right). \tag{3.1b}$$

This leap-frog scheme is stabilized by occasionally mixing three successive time-steps. In (3.1) the circumflex denotes Fourier transforms. The velocity $\boldsymbol{v}$ has components (v_1, v_2, v_3) and $\boldsymbol{\omega} = \mathrm{Curl}\,\boldsymbol{v}$ is the vorticity. $\mathbb{P}(\boldsymbol{k})$ is the projector on the space of solenoidal functions. To compute the nonlinear terms, differentiations are made on the Fourier space and multiplications in the physical space.

3.2. *Rigid boundary conditions*

We use a pseudospectral method where velocity, magnetic field and temperature are expanded in exponential Fourier series in the horizontal directions and in Chebyshev polynomial series in the vertical direction. We write

$$\vartheta(x,y,z,t) = \sum_{|l|<\frac{1}{2}L} \sum_{|m|<\frac{1}{2}M} \sum_{n=0}^{N} \vartheta_{lmn}(t) \exp\left(2i\pi\left(\frac{lx}{L_x}+\frac{my}{L_y}\right)\right) T_n(2z), \tag{3.2}$$

and similar expressions for the other fields. We use the resolutions $(L = 16, M = 10, N = 33)$ and $(L = 16, M = 16, N = 33)$.

The temporal scheme is second order Adams–Bashforth–Crank–Nicolson, of the form (same units as in (2.1))

$$\frac{\boldsymbol{v}^{n+1}-\boldsymbol{v}^n}{\delta t} = -\tfrac{1}{2}(3\boldsymbol{v}^n\cdot\nabla\boldsymbol{v}^n - \boldsymbol{v}^{n-1}\cdot\nabla\boldsymbol{v}^{n-1}) - \tfrac{1}{2}R(3\vartheta^n-\vartheta^{n-1})\boldsymbol{e}_3 + \tfrac{1}{2}Q\frac{\partial}{\partial y}(\boldsymbol{b}^n+\boldsymbol{b}^{n+1}) + \tfrac{1}{2}\nabla^2(\boldsymbol{v}^n+\boldsymbol{v}^{n+1}) - \nabla p, \tag{3.3a}$$

$$\frac{\vartheta^{n+1}-\vartheta^n}{\delta t} = -\tfrac{1}{2}(3\boldsymbol{v}^n\cdot\nabla\vartheta^n - \boldsymbol{v}^{n-1}\cdot\nabla\vartheta^{n-1}) + \frac{1}{2Pr}\nabla^2(\vartheta^n+\vartheta^{n+1}) - \tfrac{1}{2}(v_3^n+v_3^{n+1}), \tag{3.3b}$$

$$\nabla\cdot\boldsymbol{v}^{n+1} = 0, \tag{3.3c}$$

$$\nabla^2\boldsymbol{b}^{n+1} = -\frac{\partial\boldsymbol{v}^{n+1}}{\partial y}. \tag{3.3d}$$

The nonlinear terms are computed by collocation. The advective term $\boldsymbol{v}\cdot\nabla\boldsymbol{v}$ is actually replaced by

$$\frac{1}{3}\frac{\partial}{\partial x}(v_1-v_2) + \frac{1}{3}\frac{\partial}{\partial y}(v_2-v_3) + \frac{\partial}{\partial y}(v_1 v_3) + \frac{\partial}{\partial z}(v_1 v_3)$$

in the equation for $\partial v_1/\partial t$ and by analogous expressions obtained by cyclic permutations in the equations for $\partial v_2/\partial t$ and $\partial v_3/\partial t$. The pressure p must then be replaced by $p+\frac{1}{3}v^2$. By this method (Basdevant 1983) 8 Fourier transforms are needed instead of the 9 transforms required when the representation $\boldsymbol{v}\cdot\nabla\boldsymbol{v}$ or $\boldsymbol{\omega}\times\boldsymbol{v}$ is retained. Indeed, instead of computing the derivatives of v_1^2, v_2^2 and v_3^2 separately, one computes those of $v_1^2-v_2^2$ and $v_2^2-v_3^2$. The derivative of $(v_2^2-v_3^2)$ is obtained from their differences.

Time marching is done in spectral space using a tau-method (Gottlieb & Orszag 1977). The incompressibility condition (3.2*c*) leads to a Laplace equation for the pressure when we take the divergence of (3.2*a*). The resulting system for $\boldsymbol{v}^{n+1}$, $\boldsymbol{b}^{n+1}$ and p is solved as in Kleiser & Schumann (1979) by prescribing beyond (2.3) and (2.4*b*), $\nabla\cdot\boldsymbol{v}^{n+1} = 0$ for $z = = \pm\frac{1}{2}$ as an additional boundary condition required to compute the pressure. This condition ensures an exact preservation of the flow incompressibility by the temporal discretization. A similar method, referred to as the Green function method wa used by Marcus, Orszag & Patera (1984). Technical details can be found in Sulem *et al.* (1985) where preliminary results have been reported in the case of rigid boundary conditions.

4. Comparison with previous two-dimensional computations

4.1. *Free-slip boundary conditions*

It is well known that when the Rayleigh number exceeds the critical value $R_c = 27\pi^4/4$, disturbances of wavenumber $k_x = \pi/\sqrt{2}$ are amplified and convection occurs (Chandrashekhar 1961). Using a perturbative expansion in terms of $R - R_c$, Schlüter *et al.* (1965) showed that near the threshold, only two-dimensional solutions are stable. They can be represented (in diffusive units) by

$$\left.\begin{aligned} v_1 &= Ak_x^2 \pi \sin k_x x \sin \pi z + O(A^2), \\ v_2 &= 0, \\ v_3 &= A_x^2 \cos k_x \sin \pi z + O(A^2), \\ \vartheta &= \frac{A}{R}(\pi^2 + k_x^2) \cos k_x x \sin \pi z - \frac{Pr\, A}{R}(\pi^2 + k_x^2)\frac{k_x^2}{4\pi} \sin \pi z + O(A^2), \end{aligned}\right\} \tag{4.1}$$

with

$$A = \frac{\sqrt{B}(R - R_c)^{\frac{1}{2}}}{k_x(\pi^2 + k_x^2)}.$$

To test our code we have reproduced this steady two-dimensional regime, by solving numerically the time-dependent three-dimensional equation. Table 1 gives the maximum of the velocity and of the temperature derivative from the diffusive profile as predicted by Schlüter *et al.* (1965) and the value obtained numerically for $k_x = \pi/\sqrt{2}$ at different Rayleigh and Prandtl numbers. A very good agreement is obtained.

It is of interest to notice that for free-slip boundary conditions, the stability of the two-dimensional rolls that we have obtained at Prandtl number $Pr = 0.2$ is due to the small aspect ratios of the periodicity intervals that we have used. As shown by Busse & Bolton (1984) and Bolton & Busse (1985), in an infinite domain, convective rolls with critical wavenumber $k_x = \pi/\sqrt{2}$ are unstable at $Pr < 0.543$, under the action of long-wavelength instabilities which are here suppressed.

Another comparison concerns the variation of the Nusselt number with the Rayleigh number. At Prandtl number $Pr = 1$, Moore & Weiss (1973) obtained the empirical law

$$Nu = 1.9\left(\frac{R}{R_c}\right)^{0.385} \tag{4.2}$$

in the domain $5 < R/R_c < 1000$ on the basis of two-dimensional simulations. In figure 1, this scaling law is represented by the solid line. The dots are the values that we have obtained in three-dimensional calculations with a resolution of $48 \times 48 \times 24$ Fourier modes. It is remarkable that the agreement between two- and three-dimensional calculations is excellent at least up to $R \approx 80R_c$. The last point at $100R_c$ is below the curve. It is however difficult to assert that this slight discrepancy is due to three-dimensional effects, since $100R_c$ is at the limit of the Rayleigh numbers we can safely simulate with the above resolution. Note that a simple dimensional argument (Spiegel 1971) gives $Nu \sim R^{\frac{1}{3}}$ for moderate or large Prandtl numbers. The fact that the space dimensionality does not play any role in this argument can explain the good agreement obtained with two-dimensional computations.

	$R = 665$, $Pr = 0.025$		$R = 661$, $Pr = 0.1$		$R = 680$, $Pr = 0.1$	
	v_{max}	ϑ_{max}	v_{max}	ϑ_{max}	v_{max}	ϑ_{max}
Asymptotic analysis	1.642	0.0776	1.121	0.0532	2.846	0.131
Numerical calculation	1.65	0.078	1.126	0.0535	2.8	0.131

TABLE 1. Free-slip boundary conditions: comparison of the maximum velocity and maximum temperature deviation from the diffusive profile given by the asymptotic analysis of Schlüter *et al.* (1965) and by our numerical simulations (in diffusive units)

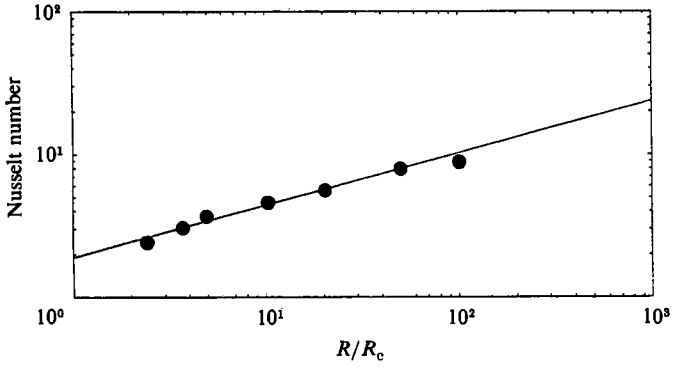

FIGURE 1. Free-slip boundary conditions, $Pr = 1$: Rayleigh-number dependence of the Nusselt number. The solid line is the scaling law (4.2). The dots are our results at a resolution of $48 \times 48 \times 24$.

Rayleigh number	$\frac{1}{2}\frac{\langle v^2 \rangle}{R - R_c}$ (thermal units)	Nusselt number
1800	1.88×10^{-3}	1.0077
1900	3.38×10^{-3}	1.0286
2000	4.83×10^{-3}	1.0606
3000	0.11	1.435

TABLE 2. Rigid boundary conditions: kinetic energy of the rolls and Nusselt number as a function of the Rayleigh number for steady two-dimensional convection at $Pr = 0.025$ and $k_y = 3.117$. The same definitions and units as in Clever & Busse (1974) have been used. For $R = 1900, 2000, 3000$, the two-dimensional rolls are only stable in the presence of a sufficiently strong magnetic field parallel to the rolls.

4.2. *Rigid boundary conditions*

In this geometry, convection occurs when the Rayleigh number exceeds the critical value $R_c = 1708$, for which disturbances of wavenumber $k_x = 3.117$ are amplified, leading to a steady state where the convective patterns are two-dimensional rolls.

This steady two-dimensional solution was computed numerically by Clever & Busse (1974, 1981) and Busse & Clever (1981) for different values of the roll wavelength and of the Rayleigh and Prandtl numbers. We have reproduced some of their results. To make quantitative comparison, we have computed (see table 2) the kinetic energy of the rolls and the Nusselt number (the ratio of the convective to the diffusive heat

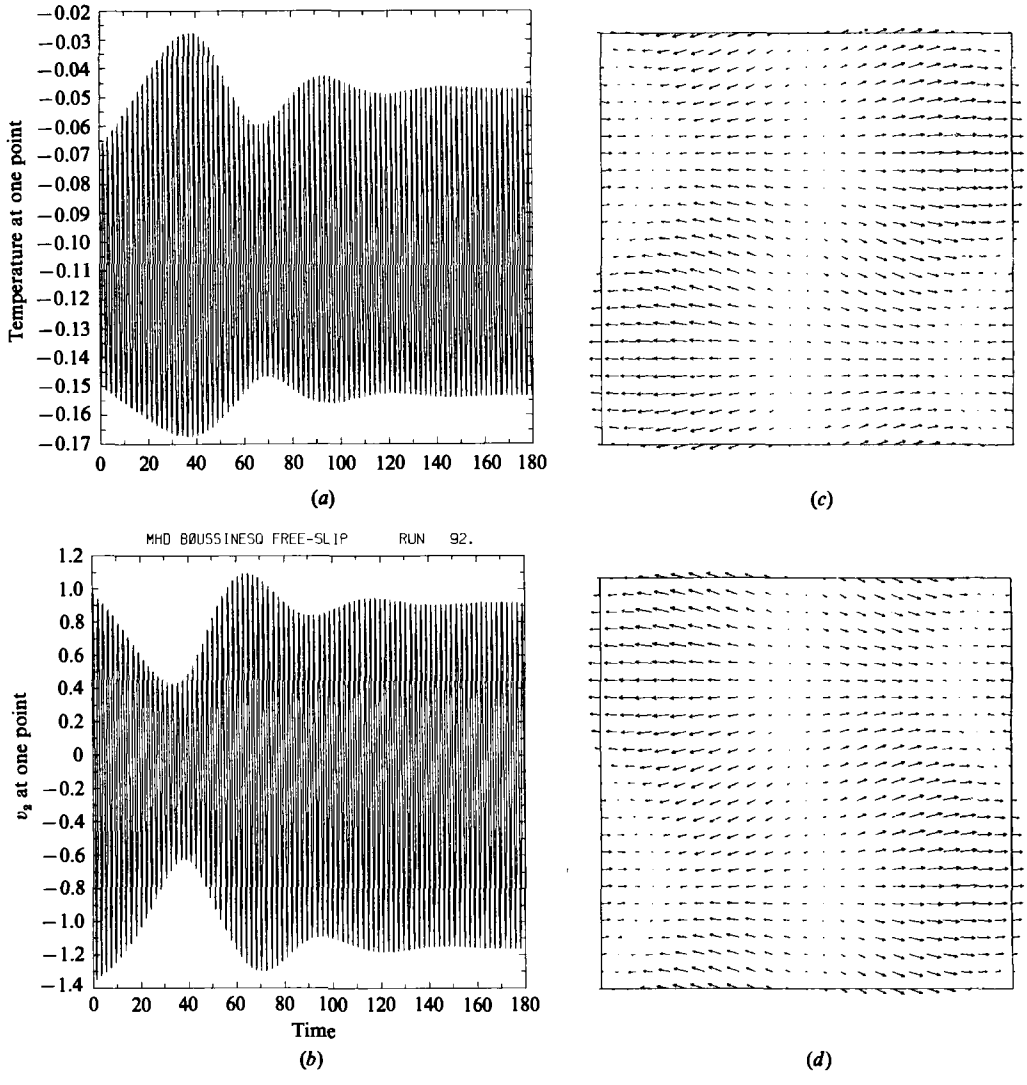

FIGURE 2. Free-slip boundary conditions, $Pr = 0.2, R = 800$. Time evolution (in diffusion time units) of (*a*) temperature ϑ and (*b*) velocity component v_2 in the roll direction at the point $(1, 1, \frac{1}{4})$ after a first transient. (*c*) Horizontal componentof the velocity at the lower boundary when the solution is time periodic. (*d*): same as (*c*) 20 diffusion times later.

transfer). The values that we have obtained are exactly on the curves presented in figure 2 of Clever & Busse (1974) and on figure 11 of Clever & Busse (1981). An agreement of better than 0.1 % is obtained with the Nusselt numbers listed in table 1 of Clever & Busse (1974).

5. Time-dependent convection with free-slip boundary conditions ($Pr = 0.2$)

When the Rayleigh number is increased, the two-dimensional rolls may become unstable. For low Prandtl numbers, the dominant effect is due to the inertial term $\boldsymbol{v}\cdot\nabla\boldsymbol{v}$ which couples vertical vorticity modes with basic two-dimensional rolls and generates the oscillatory instability. This instability corresponds to a wave propa-

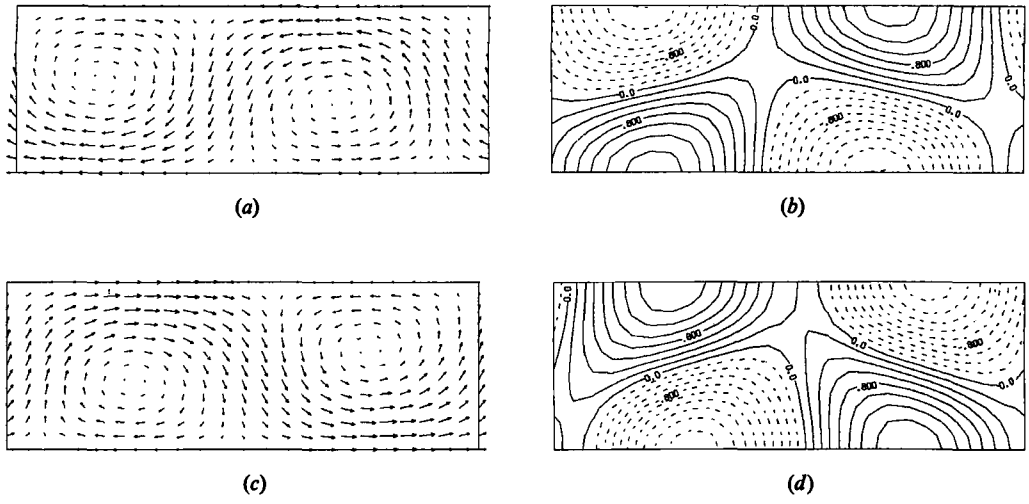

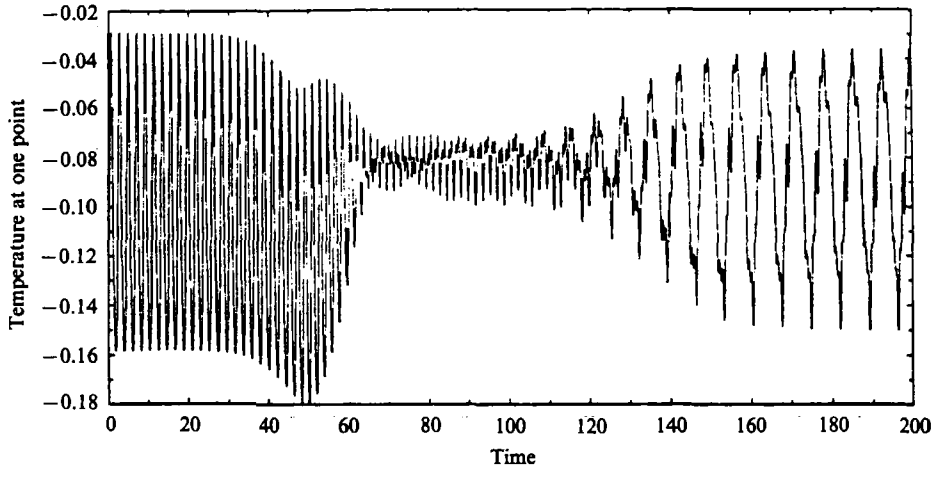

FIGURE 4. Free-slip boundary conditions, $Pr = 0.2$: transition to a two-frequency regime when R is abruptly increased from 820 to 850.

gating in the direction of the rolls. Under the conditions we have considered, we find that the threshold R_{osc} is located in the range $700 < R_{\mathrm{osc}} < 710$: For $R = 700$, we find that the two-dimensional rolls are stable while for $R = 710$, we observe the development of the instability and its saturation leading to a time-periodic solution. When the Rayleigh number is abruptly increased from $R = 700$ to 710, the temperature at a given point starts to oscillate in time, with a period of the order of the heat diffusion time. Similar behaviour is observed for the velocity components. In physical space, a travelling wave (of small amplitude because of the vicinity of R_{osc}) is seen to propagate along the rolls.

When the Rayleigh number is increased to $R = 800$, the solution is again asymptotically time periodic. Nevertheless, after a first transient during which the

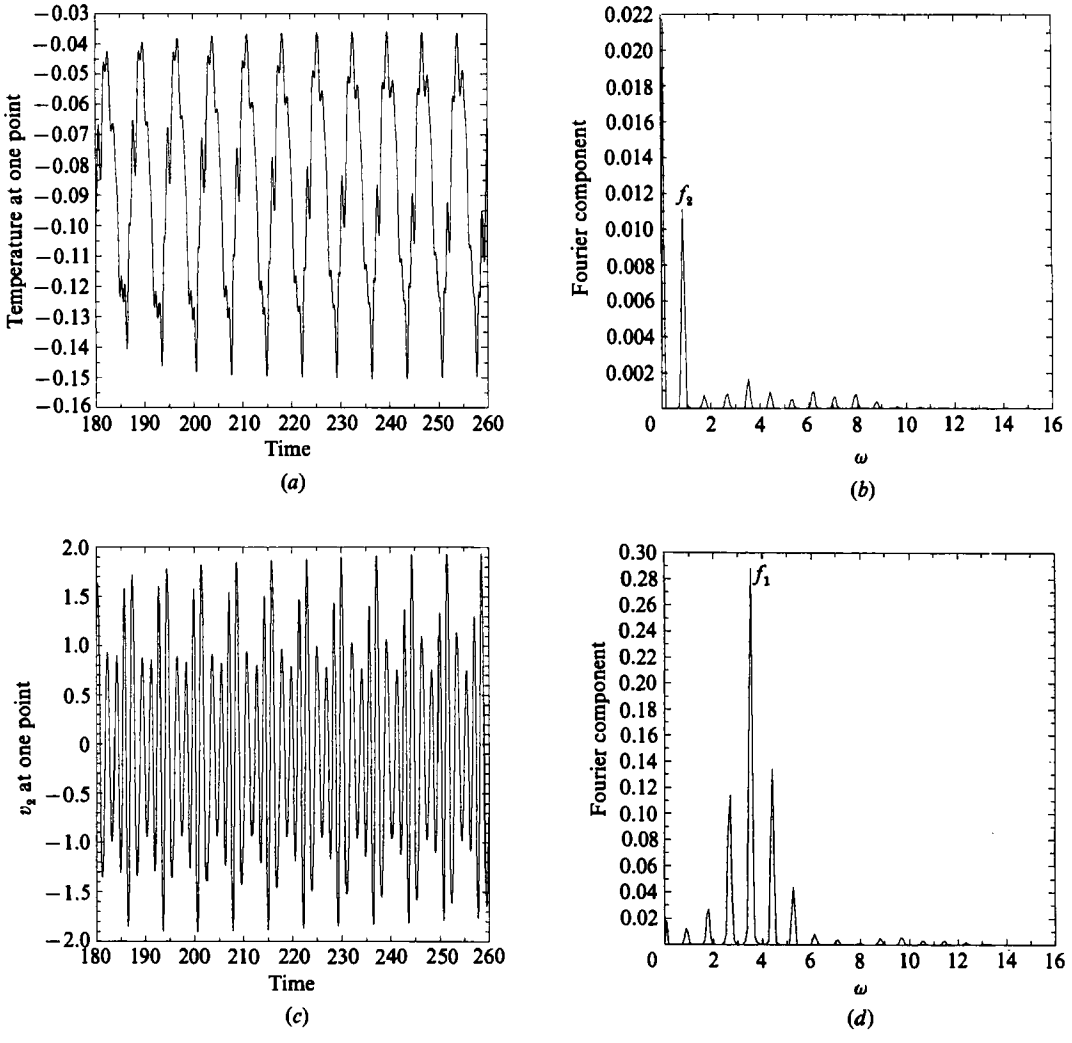

FIGURE 5. Free-slip boundary conditions, $Pr = 0.2$: almost-locked two-frequency regime ($f_1/f_2 = 4.090$) which establishes at $R = 850$: (*a*) temperature at the point $(1, 1, \frac{1}{4})$ versus time and (*b*) its temporal Fourier spectrum; (*c*) velocity component v_2 in the roll direction at the same point and (*d*) its temporal Fourier spectrum.

system adjusts itself to the new value of the Rayleigh number, we observe that during a relatively long time interval, the amplitude of the oscillation is slowly modulated, with a characteristic timescale that is about 30 times longer than the oscillation period (figure 2*a*, *b*). A similar phenomenon is also present in the case of rigid boundary conditions (see §6). In this case, the modulation has been reproduced in a model derived from phase-dynamics analysis (Brachet & Fauve 1987). Figure 2 (*c*, *d*) shows the roll oscillations in the physical space.

A very similar evolution is observed at $R = 820$. Figure 3 shows the velocity field ($(v_1 v_3)$-components and isotachs of v_2) in the plane $y = 0$. Note that the vertical oscillation of the rolls persists when the solution has become time-periodic.

A qualitatively different regime is observed when the Rayleigh number is abruptly increased from $R = 820$ to 850 (figure 4). There is a first period of time where the

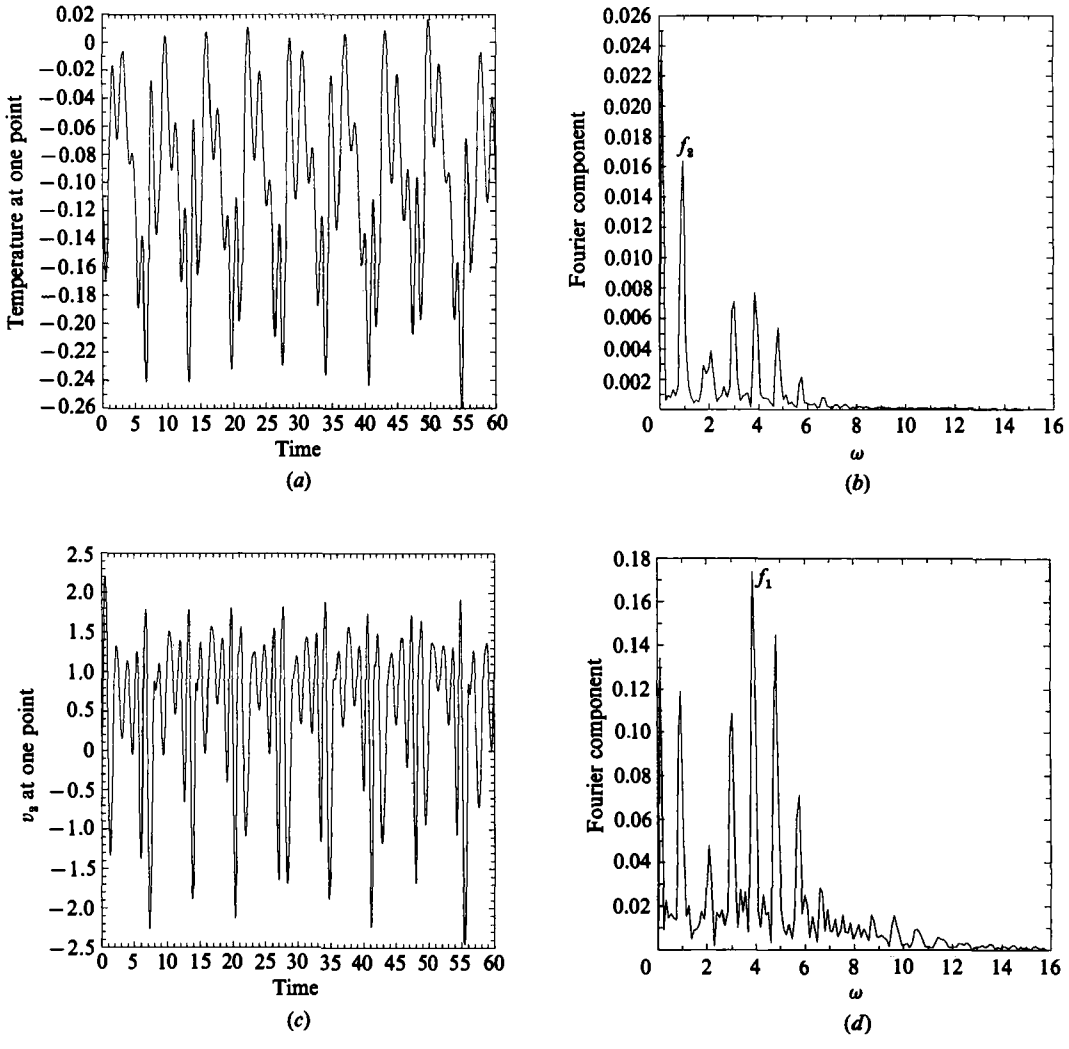

FIGURE 6. Free-slip boundary conditions, $Pr = 0.2$: Two-frequency regime ($f_1/f_2 \approx 4.17$) which establishes at $R = 900$. (*a–d*) as in figure 5.

system oscillates periodically with a frequency f_1 like at $R = 820$. It then makes a sharp transition to a regime characterized by two frequencies f_1 and f_2 which are almost locked: $f_1/f_2 \approx 4.090$. Note that f_1 is dominant in the temperature, while f_2 is dominant in the velocity component v_2 (figure 5).

When the Rayleigh number is increased to $R = 900$, we still observe a bi-periodic regime (figure 6), the ratio of the frequencies being now $f_1/f_2 \approx 4.17$.

Finally, when the Rayleigh number reaches $R = 925$, we observe a chaotic regime characterized by a broad continuous spectrum (figure 7). Note the presence of the frequency $\frac{1}{2}f_2$. This suggests that the transition to turbulence by increasing the Rayleigh number could result from the interruption of a doubling cascade of tori after a finite number of steps. This number can even be reduced to unity as in the Ginsburg–Landau equation (Kuramoto & Koga 1982; Moon, Huerre & Redekopp 1983; Keefe 1985), and in a seven-mode truncation of the incompressible Navier–

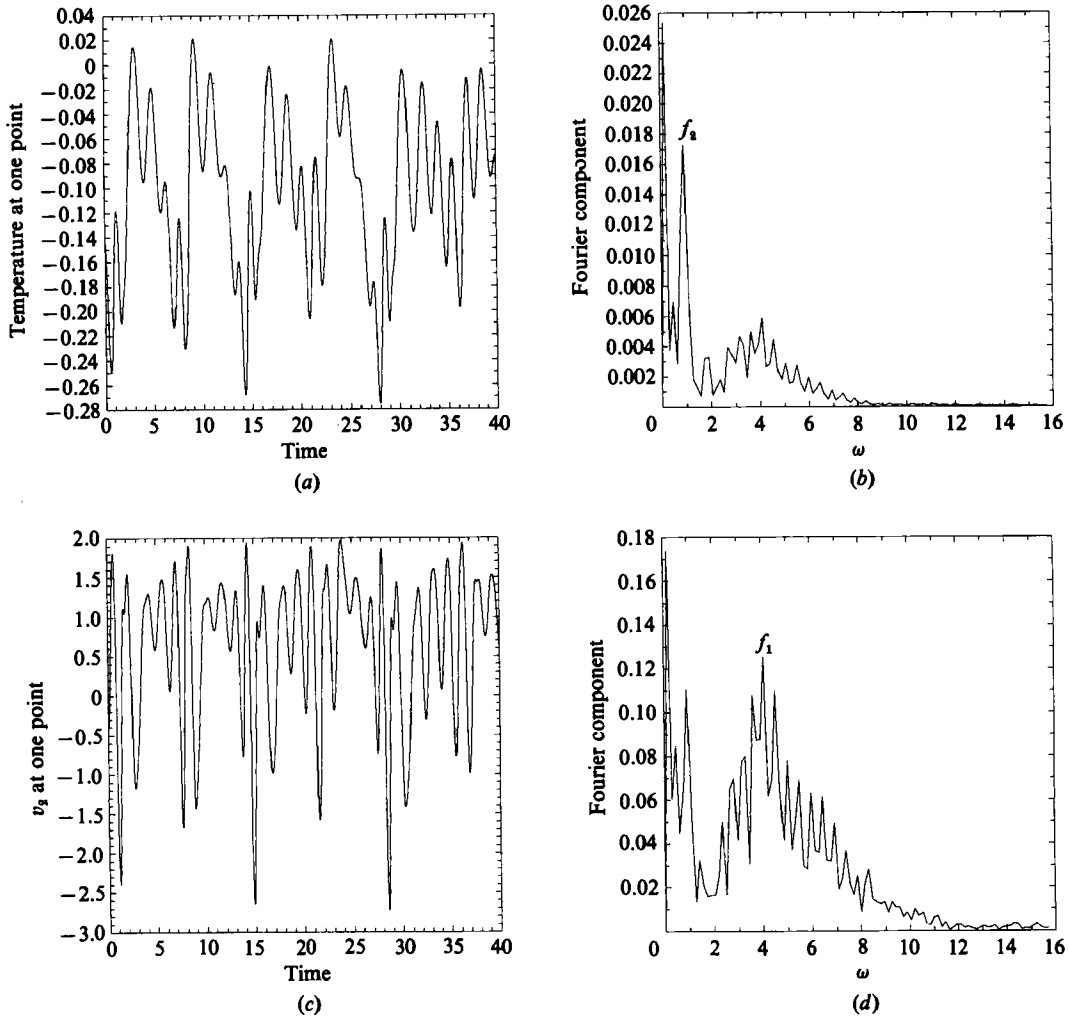

FIGURE 7. Free-slip boundary conditions, $Pr = 0.2$: Chaotic regime which establishes at $R = 925$. (*a–d*) as in figure 5.

Stokes equation (Franceschini 1983). In these examples, direct transition from a bi-periodic to a chaotic regime occurs when one of the frequency has undergone a simple period-doubling bifurcation. This incomplete cascade was shown to be a generic scenario when a system that would undergo an infinite cascade is coupled with an oscillator of different frequency (Arneodo, Coullet & Spiegel 1983; Argoul & Arneodo 1984). To clarify the relevance of this scenario to the dynamics observed in our simulations, more detailed analysis such as Poincaré sections would be required.

We finally note that comparison of figures 2, 5, 6 and 7 shows that the frequency of the oscillations increases with the Rayleigh number, a phenomenon also observed with rigid boundary conditions (§6 and Clever & Busse 1986).

The transition from periodic to chaotic dynamics is visualized in figure 8 where the temperature at the point $(1, 1, \frac{1}{4})$ is plotted versus the velocity component v_2 in the roll direction at the same point, for Rayleigh numbers of 800, 850, 900 and 925.

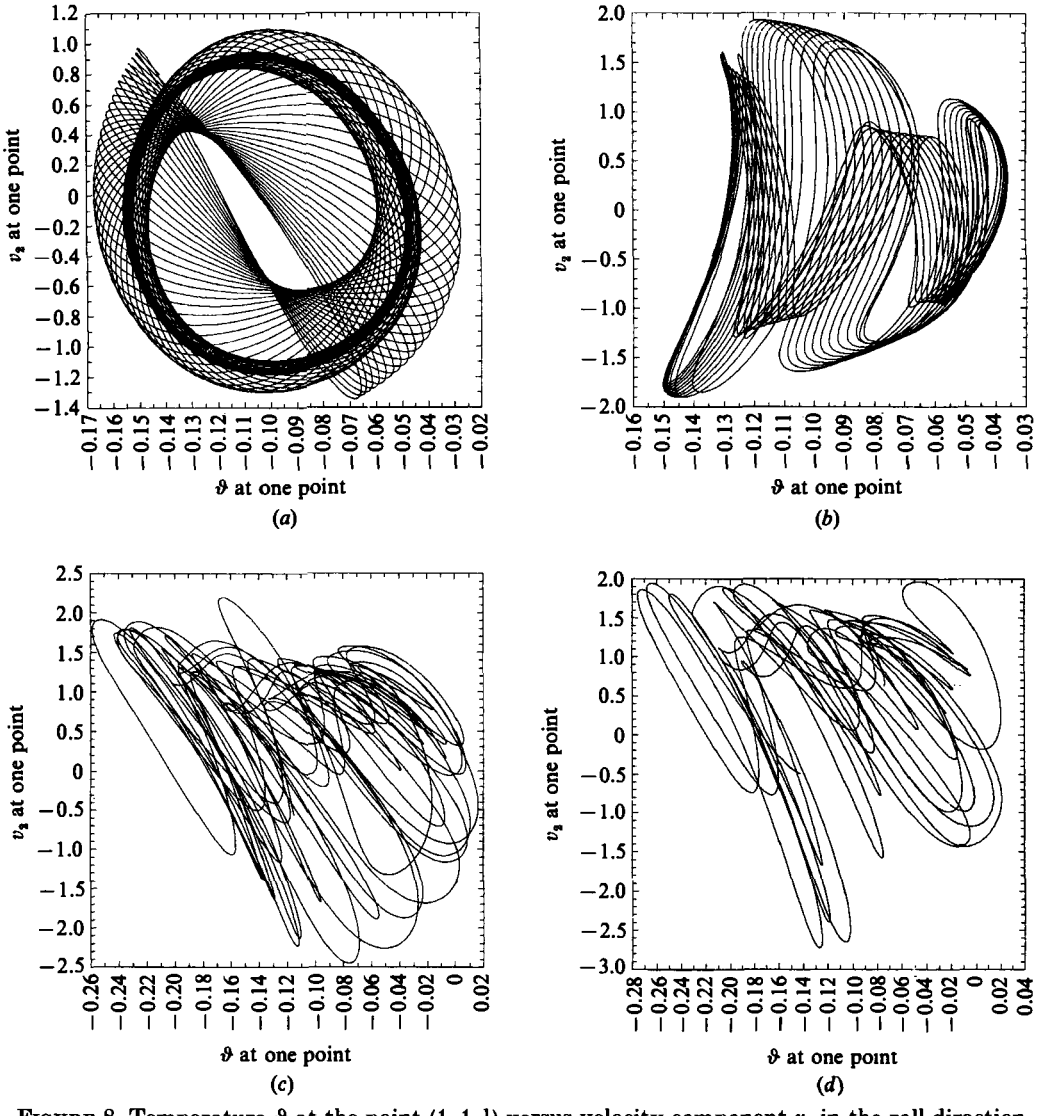

FIGURE 8. Temperature ϑ at the point $(1, 1, \frac{1}{4})$ versus velocity component v_z in the roll direction at the same point for Rayleigh numbers (*a*) 800, (*b*) 850, (*c*) 900, (*d*) 925.

6. The oscillatory instability for rigid boundary conditions ($Pr = 0.025$)

The two-dimensional rolls with basic wavenumber $k_x = 3.117$ described in §4.2 become unstable to three-dimensional disturbances at a Rayleigh number R_{osc} which strongly depends on the Prandtl number and varies slowly with the wavenumber k_y of the perturbations (Clever & Busse 1974, 1981; Busse & Clever 1981). In the case $Pr = 0.025$ and $k_y = 2.5$ that we consider here, the threshold is $R_{\text{osc}} \approx 1885$ (Busse & Clever 1983).

We start with the steady solution corresponding to two-dimensional rolls at $R = 2000$ and we destabilize it by mean of random disturbances. We measure the temperature deviation from the diffusive profile at a given point of the flow, as a function of time. We first observe a linear oscillatory regime where the amplitude

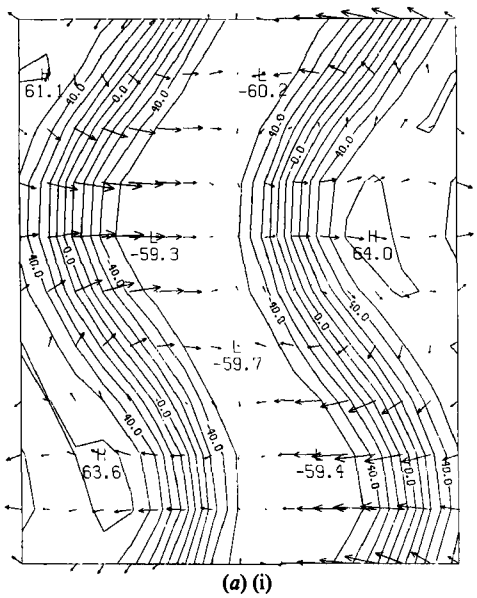

(*a*) (i)

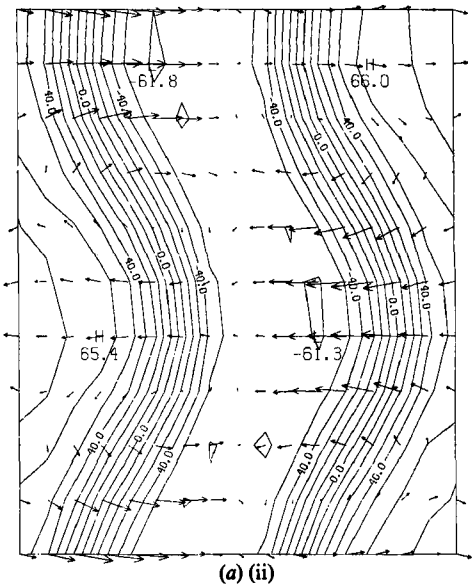

(*a*) (ii)

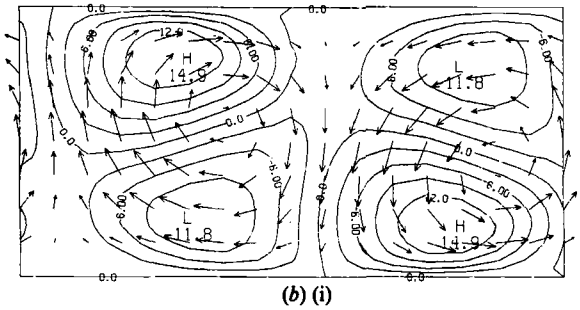

(*b*) (i)

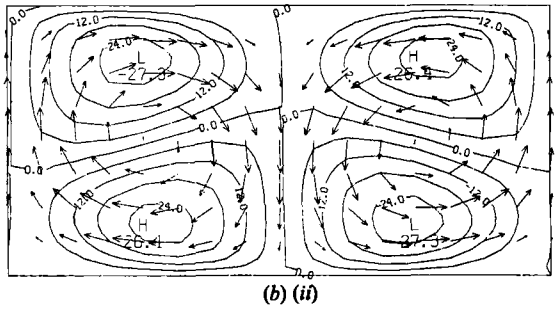

(*b*) (*ii*)

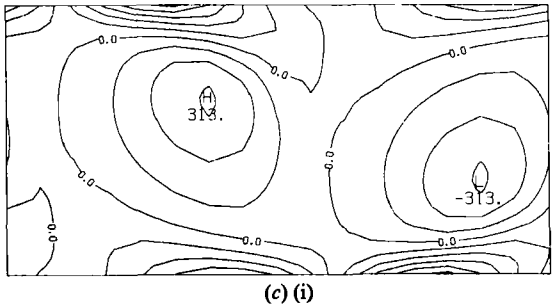

(*c*) (i)

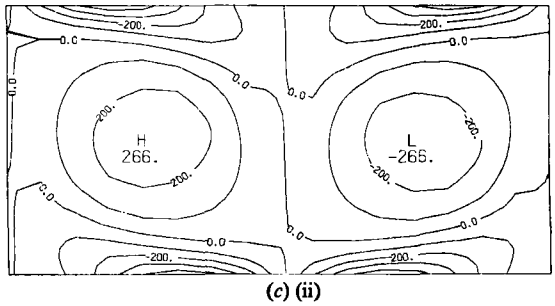

(*c*) (ii)

FIGURE 9. Rigid boundary conditions, $Pr = 0.025, R = 2000$: (*a*) (v_1, v_2)-velocity components and isotachs of v_3 in the plane $z = \frac{1}{2}$, (*b*) (v_1, v_3)-velocity components and isotachs of v_2 in the plane $y = \frac{1}{5}L_y$, (*c*) vorticity component in the roll direction in the plane $y = \frac{1}{5}L_y$. (i) Time = 1.5, (ii) 4.5.

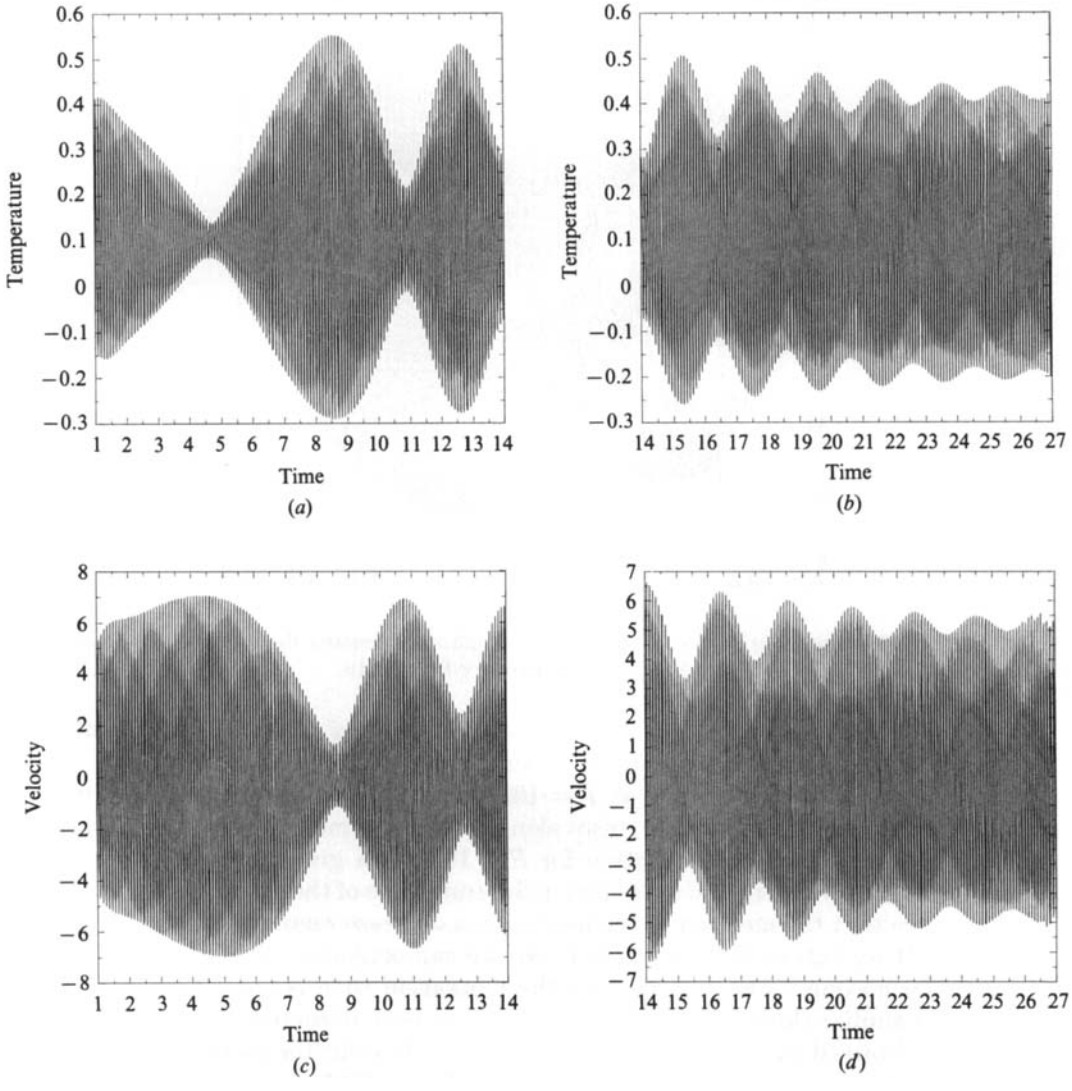

FIGURE 10. Rigid boundary conditions, $Pr = 0.025, R = 1925$: temperature ϑ at the point $(\frac{1}{4}L_x, \frac{1}{4}L_y, \frac{1}{4})$ versus time for (*a*) $1 \leqslant t \leqslant 14$ and (*b*) $14 \leqslant t \leqslant 27$. v_z component of the velocity at the same point versus time for (*c*) $1 \leqslant t \leqslant 14$ and (*d*) $14 \leqslant t \leqslant 27$.

grows exponentially. The period of the oscillation T_{osc} is about 0.065 viscous time units or equivalently 2.6 thermal diffusion time units. This corresponds to a frequency $\sigma_{\text{osc}} = 2\pi/T_{\text{osc}} \approx 2.4$ in thermal units, in agreement with figure 12 of Clever & Busse (1974). At later time, around $t = 1.5$, we see a nonlinear saturation of the amplitude. The computation, performed up to $t = 5$ (viscous units) shows a strong modulation of the amplitude on a characteristic time of about 3 viscous units. A much longer integration would be necessary to characterize the asymptotic behaviour. Figure 9 represents the velocity field and the vorticity component in the roll direction at $R = 2000$ at two different instants of time. Strong oscillations of the rolls are visible. As noticed by M. E. Brachet (private communication) the velocity field in a vertical plane (figure 9(*b*)(i), (ii)) looks very similar to that observed at the onset of the

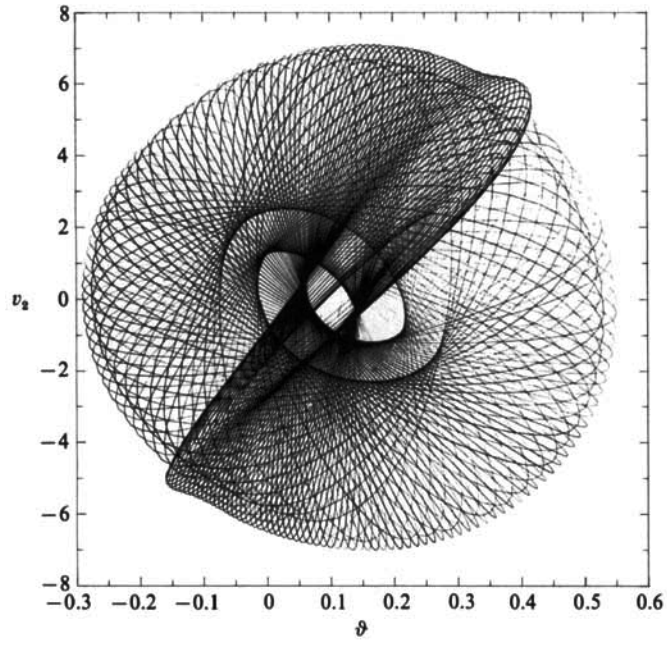

FIGURE 11. Rigid boundary conditions, $Pr = 0.025$: temperature fluctuations ϑ versus v_2 velocity component for $0 \leqslant t \leqslant 18$.

secondary instability in a plane shear flow (Brachet *et al.* 1985). We also note that the rolls display vertical undulations (figure 9(*c*)(i), (ii)).

A long calculation was done at $R = 1925$ where the integration was performed during 28 viscous time units (or equivalently 1120 thermal diffusive units) starting from the three-dimensional solution for $R = 1950$ at a given instant of time. This permits us to observe several extrema for the amplitude of the modulation (figure 10). We observe that the maxima of the modulation decrease regularly while the minima increase. If we extrapolate this behaviour, we can conjecture that the solution will eventually become time-periodic, but the relaxation time is very long. As already noticed, a similar slowly damped modulation has been observed, with an amplitude equation obtained by phase-dynamics analysis, to describe the oscillatory instability and its nonlinear saturation (M. E. Brachet & S. Fauve 1987, private communication). More quantitative comparisons are underway. In the plane (ϑ, v_2), we again obtain an ellipse which precesses, as in the similar regime with free-slip boundary conditions (figure 11).

Figure 12 shows the velocity and vorticity in physical space. The main observation is that the rolls oscillate not only horizontally but also vertically. When the Rayleigh number is reduced to $R = 1900$, we observe a weak and slow modulation. During the period $0 \leqslant t \leqslant 9$ (viscous units) during which the computation was performed, the amplitude of the oscillation of the velocity in the roll direction is increasing while that of the temperature is decreasing. At $R = 1985$, in contrast, the amplitude relaxes exponentially to a constant, leading to a time-periodic solution (figure 13).

Finally when the Rayleigh number is decreased to $R = 1880$, the oscillation of the rolls is exponentially damped. This indicates that in the conditions we have considered $1880 < R_{\mathrm{osc}} < 1895$, in agreement with the analysis of Busse & Clever (1983).

The onset of roll oscillations has experimentally been observed to reduce the

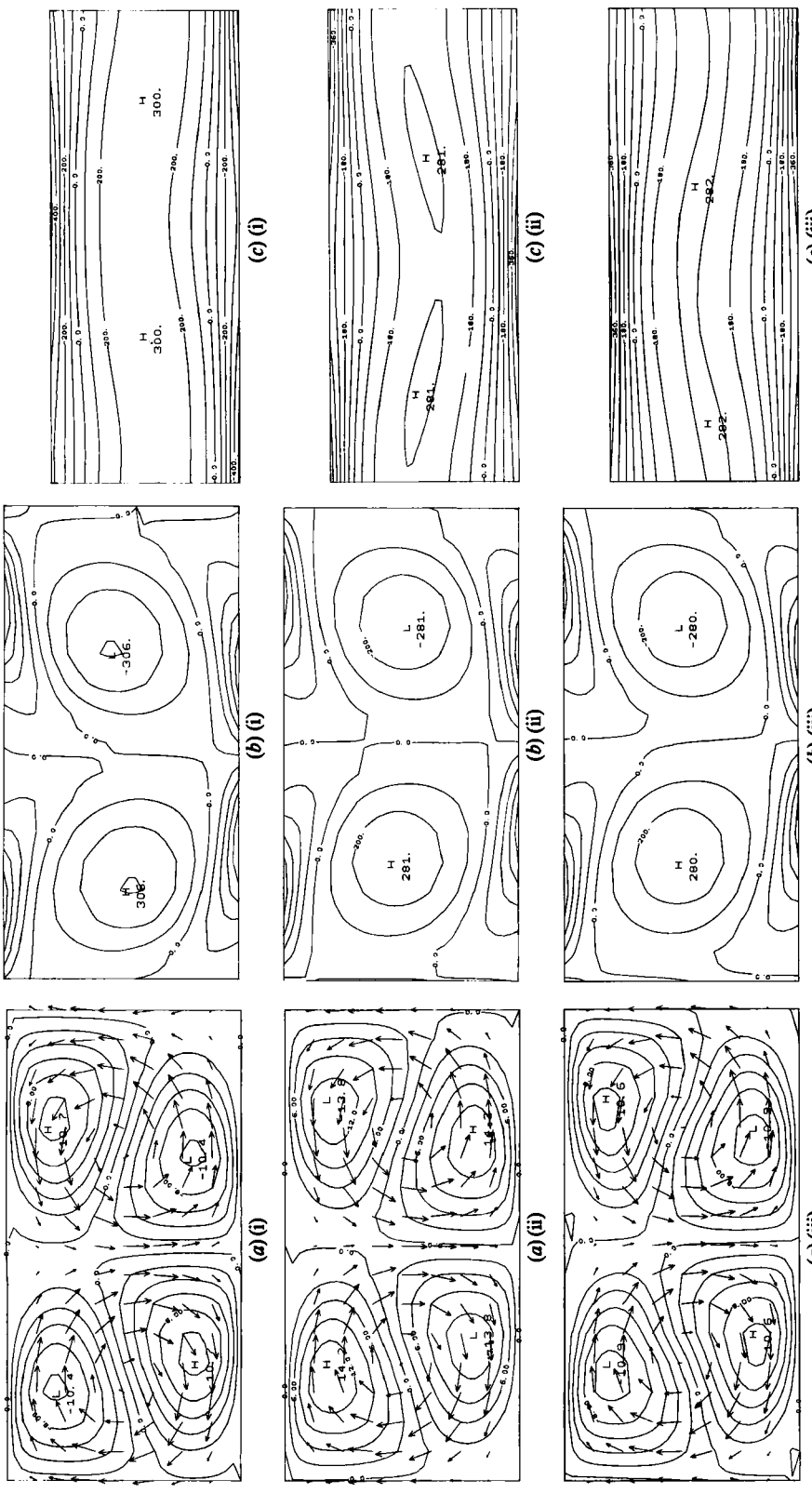

FIGURE 12. Rigid boundary conditions, $Pr = 0.025$, $R = 1925$: (*a*) (v_1, v_3)-velocity component and isotachs of v_2 in the plane $\frac{1}{8}L_y$, (*b*) vorticity component in the roll direction in the plane $y = \frac{1}{8}L_y$ and (*c*) in the plane $x = \frac{1}{4}L_x$. (i) Time = 1; (ii) 4; (iii) 11.

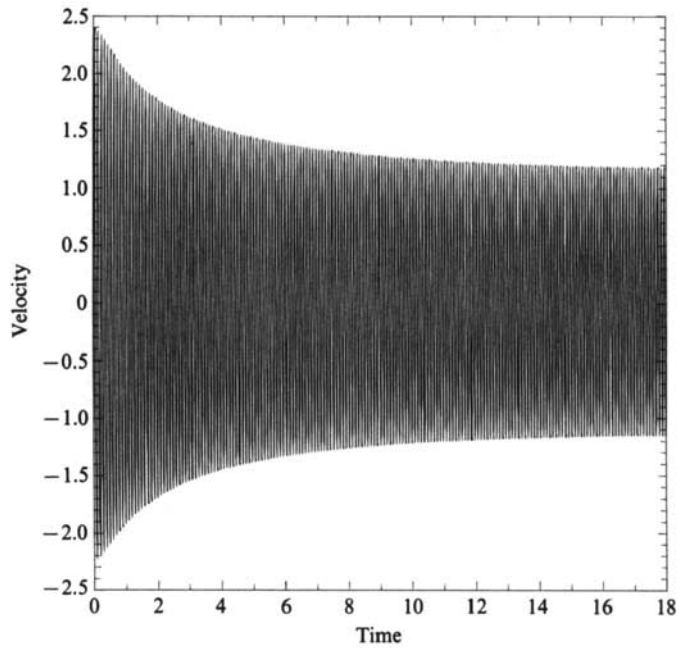

FIGURE 13. Rigid boundary conditions $Pr = 0.025, R = 1895$: velocity component in the roll direction at the point $(\frac{1}{4}L_x, \frac{1}{8}L_y, \frac{1}{4})$ as a function of time.

convective heat transfer as measured by the Nusselt number, especially at low Prandtl number (Rossby 1969; Krishnamurti 1973; Maeno, Hauche & Wheatley 1985). This effect, which has been investigated numerically by Clever & Busse (1986), is also visible in our direct simulations. For example, at $R = 2000$, the Nusselt number is $Nu \approx 1.0606$ for the two-dimensional solution while it oscillates between 1.0272 and 1.0304 for the three-dimensional solution. At $R = 1900$, $Nu = 1.0286$ for the two-dimensional solution and oscillates between 1.0270 and 1.0272 for the three-dimensional solution. As expected from symmetry arguments, the oscillation frequency of the Nusselt number is twice the basic oscillatory frequency of the roll.

7. Influence of a magnetic field parallel to the roll axis

As indicated by the linear analysis of Busse & Clever (1983), the stability region of the two-dimensional solution is enhanced by the presence of a magnetic field parallel to the roll axis. Like Busse & Clever (1983), we consider this problem for the case of rigid boundary conditions. As previously, $Pr = 0.025$, $k_x = 3.117$ and $k_y = 2.5$.

When a time-dependent flow at $R = 1900$ is abruptly subjected to a magnetic field corresponding to a Chandrashekhar number $Q = 50$, the oscillations are immediately suppressed. When $Q = 5$, we observe an essentially exponential decay of the amplitude of the oscillation without sizeable change in the frequency (figure 14). When starting with the same conditions, the external magnetic field corresponds to $Q = 0.3125$, the solution relaxes exponentially to a time-periodic solution (figure 14). This indicates that the onset of the amplitude modulation requires larger Rayleigh numbers in the presence of a magnetic field. Figure 15 displays the evolution of the temperature and velocity for $R = 2000$ and $Q = 5$. In this case the magnetic field is not sufficient to suppress the modulation.

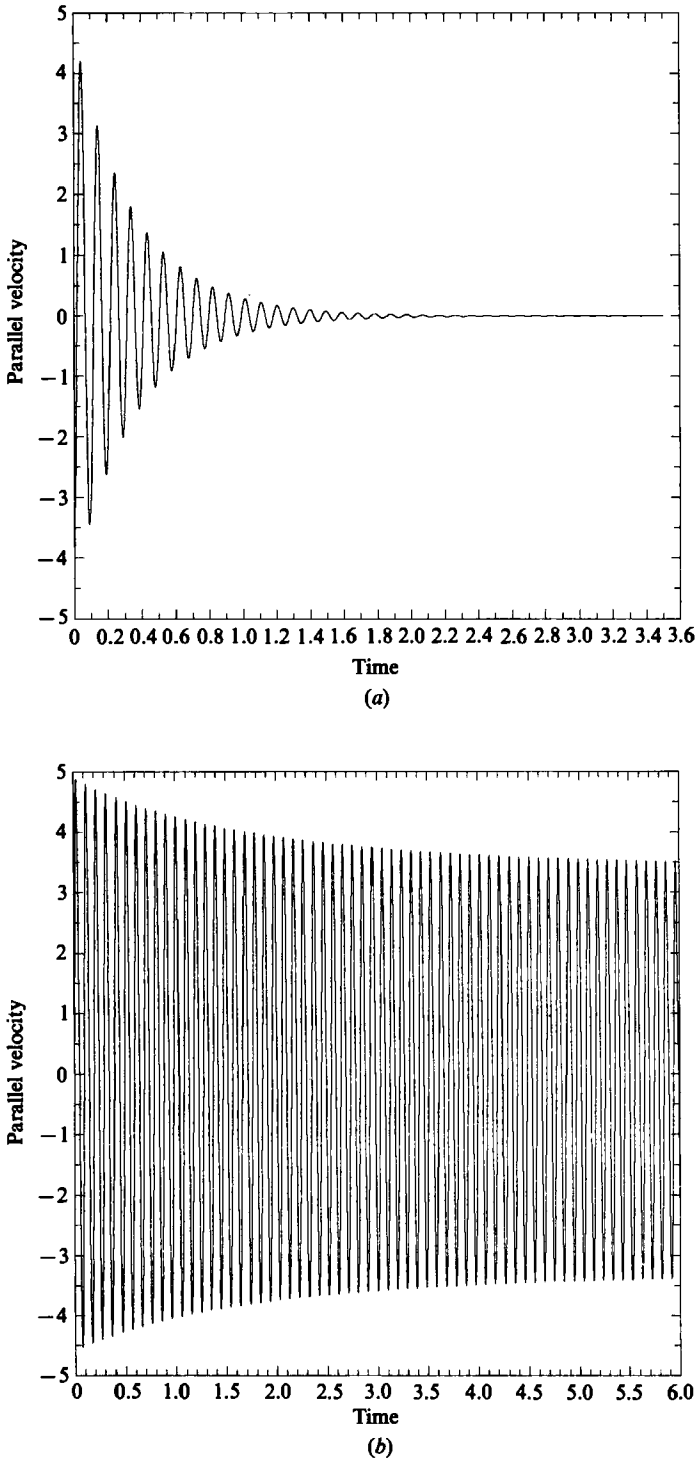

FIGURE 14. Rigid boundary conditions, $Pr = 0.025$: velocity in the roll direction versus time at $R = 1900$ in the presence of a magnetic field at the point $(\frac{1}{4}L_x, \frac{1}{5}L_y, \frac{1}{4})$: (*a*) $Q = 5$, (*b*) 0.3125.

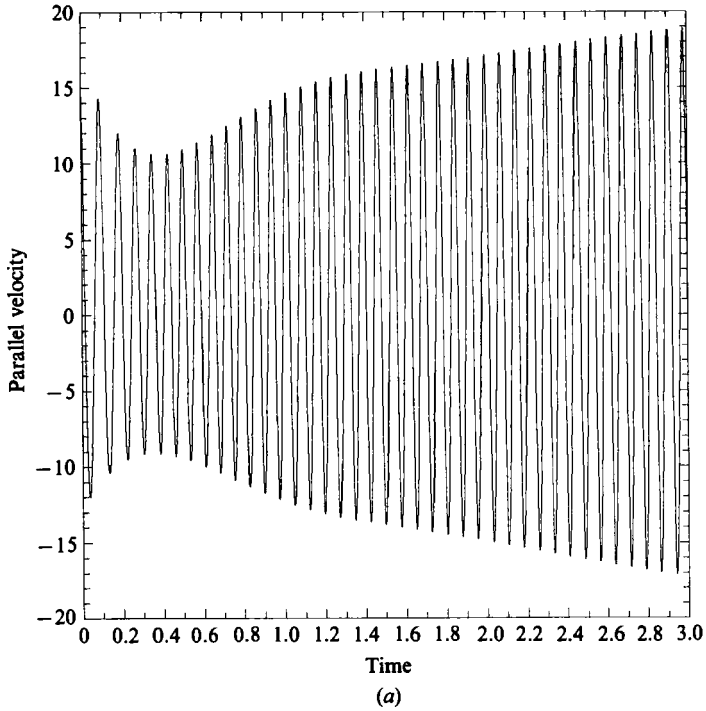

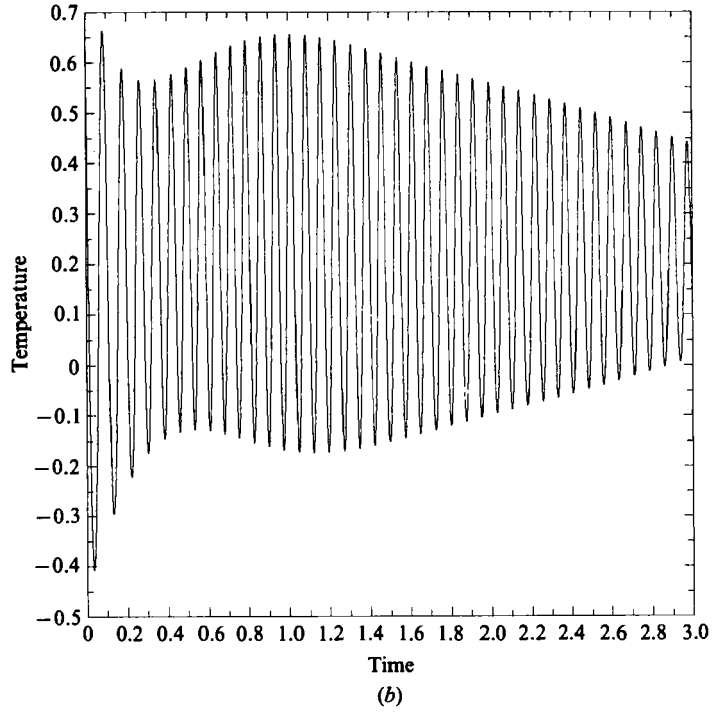

FIGURE 15. Rigid boundary conditions, $Pr = 0.025$, $R = 2000$ and $Q = 5$: (*a*) velocity in the roll direction and (*b*) temperature fluctuations at point $(\frac{1}{4}L_x, \frac{1}{5}L_y, \frac{1}{4})$ versus time.

We notice that for the oscillatory regime which is established for $R = 1900$ and $Q = 0.3125$, the Nusselt number oscillates between 1.0279 and 1.0280, values located between the Nusselt number of the two-dimensional solution and that of the three-dimensional solution for $Q = 0$. Similarly for $R = 2000$ and $Q = 5$, the Nusselt number oscillates between 1.0455 and 1.0473, again between the values of the Nusselt of the two-dimensional solution and of the three-dimensional solution for $Q = 0$. Similar observations are made for other values of the parameters: for $R = 1950$ and $Q = 5$, $Nu \approx 1.0436$ (very small oscillations) while $1.0268 \leqslant Nu \leqslant 1.0286$ for $Q = 0$. This clearly indicates that the inhibition of the oscillation by the magnetic field increases the convective heat transport.

In conclusion, for the Rayleigh numbers and the geometry that we have considered, a magnetic field in the roll direction produces no drastic modification of the dynamics. It inhibits the oscillation of the rolls and its effect may thus be viewed as essentially equivalent to a reduction of the Rayleigh number. In particular, we have not seen the onset of new bifurcations. The reason is probably that all the computations were done at Rayleigh numbers not larger than $1.2R_c$. In this range of parameters, time-dependent solutions can persist only for very moderate Chandrashekhar numbers. We cannot exclude the possibility that, as in the experiments, new scenarios would occur at sensibly larger Rayleigh and Chandrashekhar numbers, but such simulations would require larger computational power, since the resolution has to be increased accordingly.

8. Concluding remarks

One of the main difficulties in the numerical simulation of convection at very small Prandtl number is the high rotation velocity of the fluid particles. This imposes a drastic constraint on the time-step to ensure stability when an explicit scheme is used for the (nonlinear) advection terms. This makes calculations at high Rayleigh numbers prohibitively expensive in computer time, more especially as the spatial resolution has to be increased with the Rayleigh number, which also requires a reduction of the time-step. Furthermore, the transients appear to be extremely long. As a consequence, we have only simulated the first time-dependent regimes in the case of rigid boundary conditions at $Pr = 0.025$.

From this point of view, the situation was better in the simulation that we did with free-slip conditions, probably because we used a sensibly larger Prandtl number ($Pr = 0.2$). In this case, we observed a transition to chaos from a biperiodic regime with a single period-doubling bifurcation. It is of interest to notice that in the numerical simulations (which all assume periodicity in the horizontal direction), a complete cascade of period doubling was not observed. This suggests that in the experiments in helium (Libchaber & Maurer 1980) or in mercury (Libchaber *et al.* 1983), where this scenario was observed, an important role is played by the boundaries.

Note that in both the computations we have found an oscillatory solution with an amplitude that is slowly modulated. In the computations reported here this modulation is subcritical in the sense that it is eventually damped, the system relaxing to a purely periodic solution. This transient is however much longer in the case of rigid boundary conditions. It is quite possible that for slightly different values of the parameters, this modulation would be persistent, leading to a mode-softening transition to chaos as observed experimentally by Libchaber *et al.* (1983) in the presence of a magnetic field or even in its absence (S. Fauve, private communications).

Such a modulation was also observed by Curry *et al.* (1984) in simulations of two-dimensional convective flows and has been measured in the wake of a circular cylinder at Reynolds number $Re = 66$ (Sreenivasan 1985).

We have benefited from numerous discussions with S. Fauve during different stages of this work. We also acknowledge many helpful conversations with A. Arneodo, M. E. Brachet, P. Coullet, U. Frisch, J. Herring, P. Huerre, A. Libchaber, S. A. Orszag and E. Spiegel. The computations were done on the CRAY1S of the Centre de Calcul Vectoriel pour la Recherche (Palaiseau), using the fast Fourier transforms of S. A. Orszag and C. Temperton, and the NCAR Graphic Software. We have also benefited from partial support from DRET and ATP (CNRS) contracts.

REFERENCES

ARGOUL, F. & ARNEODO, A. 1984 *J. Méc. Théor. Appl.* numéro speciale, p. 241.

ARNEODO, A., COULLET, P. H. & SPIEGEL, E. A. 1983 *Phys. Lett.* **94A**, 1.

BASDEVANT, C. 1983 *J. Comp. Phys.* **50**, 209–214.

BOLTON, E. W. & BUSSE, F. H. 1985 *J. Fluid Mech.* **150**, 487.

BRACHET, M. E., METCALFE, R. W., ORSZAG, S. A. & RILEY, J. J. 1985 In *Progress and Supercomputing in Computational Fluid Mechanics. Proc. U.S. Israel Workshop 1984* (ed. E. M. Murman & S. Abarbane), p. 257. Birkhäuser.

BUSSE, F. H. 1972 *J. Fluid Mech.* **52**, 97.

BUSSE, F. H. & BOLTON, E. W. 1984 *J. Fluid Mech.* **146**, 115.

BUSSE, F. H. & CLEVER, R. M. 1981 *J. Fluid Mech.* **102**, 75.

BUSSE, F. H. & CLEVER, R. M. 1983 *J. Méc. Théor Appl.* **2**, 495.

CHANDRASHEKHAR, S. 1961 *Hydrodynamics and Magnetohydrodynamics Stability*. Oxford University Press.

CLEVER, R. M. & BUSSE, F. H. 1974 *J. Fluid Mech.* **65**, 625.

CLEVER, R. M. & BUSSE, F. H. 1981 *J. Fluid Mech.* **102**, 61.

CLEVER, R. M. & BUSSE, F. H. 1986 Nonlinear oscillatory convection. Preprint.

CURRY, J. H., HERRING, J. H., LONCARIC, J. & ORSZAG, S. A. 1987 *J. Fluid Mech.* **147**, 1.

FRANCESCHINI, V. 1983 *Physica* **6D**, 285.

GOTTLIEB, D. & ORSZAG, S. A. 1977 *Numerical Analysis of Spectral Methods: Theory and Applications*. NSF-CENS Monograph, vol. **26**. Philadelphia: Soc. Indus. Appl. Math.

HERRING, J. R. & JACKSON, S. 1984 *Turbulence and Chaotic Phenomena in Fluids* (ed. T. Tatsumi). IUTAM.

KEEFE, L. R. 1985 *Stud. Appl. Maths* **73**, 91.

KLEISER, L. & SCHUMANN, U. 1979 Treatment of incompressibility and boundary conditions in three dimensions. Numerical simulations of plane channel flows. *Notes on Num. Fluids Mech.* vol. 2 (ed. E. H. Hirschel). Proc. in Fluid Mech, DFVLR, Cologne.

KRISHNAMURTI, R. 1973 *J. Fluid Mech.* **60**, 285.

KURAMOTO, Y. & KOGA, S. 1982 *Phys. Lett.* **92A**, 1.

LIBCHABER, A., FAUVE, S. & LAROCHE, C. 1983 *Physica* **7D**, 73.

LIBCHABER, A. & MAURER, J. 1980 *J. Phys. Paris* **41**, 51.

LIPPS, F. B. 1976 *J. Fluid Mech.* **75**, 113.

MAENO, Y., HAUCHE, H. & WHEATLEY, J. C. 1985 *Phys. Rev. Lett.* **54**, 340.

MARCUS, P. S. 1981 *J. Fluid Mech.* **103**, 241.

MARCUS, P. S., ORSZAG, S. A. & PATERA, A. T. 1982 In *Proc. 8th Intl Conf. on Numerical Methods in Fluid Mechanics* (ed. E. Krause), Lecture Notes in Physics, vol. 170, p. 371. Springer.

MCLAUGHLIN, J. & ORSZAG, S. A. 1982 *J. Fluid Mech.* **122**, 123.

MOON, H. T., HUERRE, P. & REDEKOPP, L. G. 1983 *Physica* **7D**, 135.

MOORE, D. R. & WEISS, N. O. 1973 *J. Fluid Mech.* **58**, 289.

ORSZAG, S. A. & KELLS, L. C. 1980 *J. Fluid Mech.* **95**, 159.

PATERA, A. 1984 *J. Comp. Phys.* **54**, 468.

ROBERTS, P. H. 1967 *An Introduction to Magnetohydrodynamics.* Longman.

ROSSBY, H. T. 1969 *J. Fluid Mech.* **36**, 309.

RUELLE, D., TAKENS, F. & NEWHOUSE, S. 1978 *Communs Math. Phys.* **64**, 35.

SCHÜLTER, A., LORTZ, D. & BUSSE, F. 1965 *J. Fluid Mech.* **23**, 129.

SIGGIA, E. D. & ZIPPELIUS, A. 1981 *Phys. Rev. Lett.* **47**, 835.

SPIEGEL, E. A. 1971 *Ann. Rev. Astro. Astrophys.* **9**, 323.

SREENIVASAN, R. K. 1985 In *Frontiers in Fluid Mechanics* (ed. S. H. Davis & J. L. Lumley), p. 41. Springer.

SULEM, P. L., SULEM, C. & THUAL, O. 1985 In *Single and Multi-Phase Flows in an Electromagnetic Field. Proc. 4th Beersheva Seminar 1984* (ed. H. Branover, P. S. Lykoudis & M. Mond). *Prog. Astro. Aeronaut.* **100**, 125.

TREVE, Y. M. & MAULY, O. P. 1982 *Physica* **4D**, 319.

ZIPPELIUS, A. & SIGGIA, E. D. 1982 *Phys. Rev.* **A26**, 1788.

ZIPPELIUS, A. & SIGGIA, E. D. 1983 *Phys. Rev.* **A26**, 2905.